Thickness-dependent crystallization on thermal anneal for titania/silica nm-layer composites deposited by ion beam sputter method

Huang-Wei Pan,[1] Shun-Jin Wang,[1] Ling-Chi Kuo,[1] Shiuh Chao,[1,*] Maria Principe,[2,3] Innocenzo M. Pinto,[2,3] and Riccardo DeSalvo,[2,3]

[1] *Institute of Photonics Technologies and E.E. Dept., National Tsing Hua University, Hsinchu, Taiwan*
[2] *University of Sannio, Corso Garibaldi 107, Benevento, Italy*
[3] *INFN Sez.di Napoli, Italy*
[*] *schao@ee.nthu.edu.tw*

Abstract: Crystallization following thermal annealing of thin film stacks consisting of alternating nm-thick titania/silica layers was investigated. Several prototypes were designed, featuring a different number of titania/silica layer pairs, and different thicknesses (in the range from 4 to 40 nm, for the titania layers), but the same nominal refractive index (2.09) and optical thickness (a quarter of wavelength at 1064 nm). The prototypes were deposited by ion beam sputtering on silicon substrates. All prototypes were found to be amorphous as-deposited. Thermal annealing in air at progressive temperatures was subsequently performed. It was found that the titania layers eventually crystallized forming the anatase phase, while the silica layers remained always amorphous. However, progressively thinner layers exhibited progressively higher threshold temperatures for crystallization onset. Accordingly it can be expected that composites with thinner layers will be able to sustain higher annealing temperatures without crystallizing, and likely yielding better optical and mechanical properties for advanced coatings application. These results open the way to the use of materials like titania and hafnia, that crystallize easily under thermal anneal, but ARE otherwise promising candidate materials for HR coatings necessary for cryogenic 3rd generation laser interferometric gravitational wave detectors.

©2014 Optical Society of America

OCIS codes: (310.4165) Multilayer design; (310.6860) Thin films, optical properties; (160.4670) Optical materials

References and links

1. W. H. Wang and S. Chao, "Annealing effect on ion-beam-sputtered titanium dioxide film," Opt. Lett. **23**(18), 1417–1419 (1998).
2. C. C. Lee and C. J. Tang, "TiO_2--Ta_2O_5 composite thin films deposited by radio frequency ion-beam sputtering," Appl. Opt. **45**(36), 9125–9131 (2006).
3. G. Harry, A. Gretarsson, P. Saulson, S. Kittelberger, S. Penn, W. J. Startin, S. Rowan, M. M. Fejer, D. R. M. Crooks, G. Cagnoli, J. Hough, and N. Nakagawa, "Thermal noise in interferometric gravitational wave detectors due to dielectric optical coatings," Class. Quantum Gravity **19**(5), 897–917 (2002).
4. N. Nakagawa, A. M. Gretarsson, E. K. Gustafson, and M. M. Fejer, "Thermal noise in half-infinite mirrors with nonuniform loss: A slab of excess loss in a half-infinite mirror," Phys. Rev. D Part. Fields **65**(10), 102001 (2002).
5. Yu. Levin, "Internal thermal noise in the LIGO test masses: A direct approach," Phys. Rev. D Part. Fields **57**(2), 659–663 (1998).
6. S. Penn, "Exploring Coating Thermal Noise via Loss in Fused Silica Coatings," Proc. Amaldi 2009,LIGO Document G0900600, URL: https://dcc-lho.ligo.org/public/0003/G0900600/001/PennAmaldiPoster.pdf.
7. S. Chao, W. H. Wang, M.-Y. Hsu, and L.-C. Wang, "Characteristics of ion-beam-sputtered high-refractive-index TiO_2-SiO_2 mixed films," J. Opt. Soc. Am. A **16**(6), 1477 (1999).

8. O. Stenzel, S. Wilbrandt, S. Yulin and N. Kaiser et al., “Plasma ion assisted deposition of hafnium dioxide using argon and xenon as process gases,” Opt. Mater. Express. **1**(2), 278–292 (2011). The value provided in the text is a fiducial value, extrapolated from a Sellmeyer fit of results in [8]. Measured values reported in the literature for hafnia thin films vary largely, depending on the actual deposition process [9].
9. W. Ai and S. Xiong, “Characterization of hafnia thin films made with different deposition technologies,” Proc. SPIE **8190**, 81900J (2011).
10. M. R. Abernathy, S. Reid, E. Chalkley, R. Bassiri, I. W. Martin, K. Evans, M. M. Fejer, A. Gretarsson, G. M. Harry, J. Hough, I. MacLaren, A. Markosyan, P. Murray, R. Nawrodt, S. Penn, R. Route, S. Rowan, and P. Seidel, “Cryogenic mechanical loss measurements of heat treated hafnium dioxide,” Class. Quantum Gravity **28**(19), 195017 (2011).
11. W. W. Scott and R. K. MacCrone, “Apparatus for mechanical loss measurements in low loss materials at audio frequencies and low temperatures,” Rev. Sci. Instrum. **39**(6), 821 (1968).
12. F. L. Mart’ınez, M. Toledano-Luque, J. J. Gand’ıa, J. C’arabe, W. Bohne, *et al*., “Optical properties and structure of HfO_2 thin films grown by high pressure reactive sputtering,” Appl. Phys. (Berl.) **40**, 5256–5265 (2007).
13. M. Abernathy, F. Acernese, P. Ajith, B. Allen, and P. Amaro-Seoane, *Einstein Gravitational Wave Telescope Conceptual Design Study* (European Gravitational Observatory,2011).
14. K. Somiya, “Detector configuration of KAGRA–the Japanese cryogenic gravitational-wave detector,” Class. Quantum Gravity **29**(12), 124007 (2012).
15. I. W. Martin, H. Armandula, C. Comtet, M. M. Fejer, A. Gretarsson, G. Harry, J. Hough, J.-M. M. Mackowski, I. MacLaren, C. Michel, J.-L. Montorio, N. Morgado, R. Nawrodt, S. Penn, S. Reid, A. Remillieux, R. Route, S. Rowan, C. Schwarz, P. Seidel, W. Vodel, and A. Zimmer, “Measurement of a low temperature mechanical dissipation peak in a single layer of Ta_2O_5 doped with TiO_2,” Class. Quantum Gravity **25**(5), 055005 (2008).
16. I. W. Martin, R. Bassiri, R. Nawrodt, M. M. Fejer, A. Gretarsson, E. Gustafson, G. Harry, J. Hough, I. MacLaren, S. Penn, S. Reid, R. Route, S. Rowan, C. Schwarz, P. Seidel, J. Scott, and A. L. Woodcraft, “Effect of heat treatment on mechanical dissipation in Ta_2O_5 coating,” Class. Quantum Gravity **27**(22), 225020 (2010).
17. B. J. Pond, J. I. Debar, C. K. Carniglia, and T. Raj, “Stress reduction in ion beam sputtered mixed oxide films,” Appl. Opt. **28**(14), 2800–2805 (1989).
18. S. Chao, W. H. Wang, and C. C. Lee, “Low-loss dielectric mirrors with ion beam sputtered TiO_2/ SiO_2 mixed films,” Appl. Opt. **40**(13), 2177–2182 (2001).
19. S. V. Ushakov, A. Navrotsky, Y. Yang, S. Stemmer, K. Kukli, M. Ritala, M. A. Leskelä, P. Fejes, A. Demkov, C. Wang, B.-Y. Nguyen, D. Triyoso, and P. Tobin, “Crystallization in hafnia and zirconia based systems,” Phys. Status Solidi, B Basic Res. **241**(10), 2268–2278 (2004).
20. I. Martin, *et al*., “Mech Loss of Crystalline and Amorphous Coatings,” Proc. GWADW 2014, URL: *http://www.gravity.ircs.titech.ac.jp/GWADW2014/slide/Iain_Martin.pdf*.
21. H. Sankur and W. Gunning, “Crystallization and diffusion in composite TiO_2/ SiO_2 thin films,” J. Appl. Phys. **66**(10), 4747 (1989).
22. M. Liu, G. He, L. Q. Zhu, Q. Fanga, G. H. Li, and L. D. Zhang, “Microstructure and Interfacial Properties of HfO_2/ Al_2O_3 Nanolaminate Films,” Appl. Surf. Sci. **252**(18), 6206–6211 (2006).
23. I. M. Pinto, “nm Layered Coatings: Status and Perspectives” Proc. ELiTES 2nd General Meeting, URL: *http://events.ego-gw.it/indico/getFile.py/access?contribId=25&sessionId=3&resId=0&materialId=slides&confId=7*.
24. W. J. Huang, “Preparation of the ion beam sputter coater for coating the low loss thin films in LIGO mirror application,” master thesis, National Tsing Hua University Taiwan R.O.C, (2012).

1. Introduction

Thermal annealing is a common practice to improve features of optical coating quality like absorption [1] and internal stress [2]. The requirements of laser interferometric detectors of gravitational waves (henceforth GW), has given progressively more importance to the thermal noise figure of merit in dielectric mirror coatings [3–5]. It was found that thermal annealing also reduces coating mechanical losses, and hence thermal noise [6]. However, excessive thermal annealing eventually leads to crystallite growth [7]. Mechanical losses due to friction among crystallites, as well as scattering from the grain boundaries, make the coatings unsuitable. This is notably true for TiO_2 (n = 2.32 @ 1064nm) and HfO_2 (n = 1.58-1.85 @ 1064nm) [8,9] that in their amorphous state have low mechanical losses down to 10K [10–12], and have been indicated as prime choice materials for the next generation of cryogenic GW interferometers [13,14]. This is a significant advantage over presently used SiO_2 and Ta_2O_5 whose performance is spoiled by a mechanical loss peak in the cryogenic regime [15,16]. Finding ways to raise the crystallization temperature (and/or dwell time) in titania and hafnia is therefore an urgent issue.

#224393 - $15.00 USD Received 6 Oct 2014; revised 8 Nov 2014; accepted 10 Nov 2014; published 20 Nov 2014
(C) 2014 OSA

Alloying these materials with glass formers like silica or alumina in the deposition phase (co-sputtering) has been proved to be effective [10,17–19]. Notably, silica doping does not spoil the nice cryogenic properties of hafnia [20]. Pioneering work by Sankur and Gunnig [21] has shown that thin-film stacks consisting of alternating nm-scale titania/silica layers can be annealed to fairly large temperatures without significant crystallite growth. Similar findings have been more recently reported for thin film stacks consisting of alternating nm-thick hafnia/alumina layers [22]. Layered composites are easier to model than co-sputtered materials, and may be intrinsically less noisy, as suggested by a simple effective-medium theory [23].

We present a detailed study of the crystallization threshold temperature in silica/titania nm-layered composites as a function of sub-layer thickness. All films tested have the same nominal refraction index (2.09) and optical thickness (a quarter of wavelength at 1064 nm) but sub-layer thicknesses ranging from 4 to 40 nm for the titania, the thickness of the silica sub-layers and the number of sub-layers following from the prescribed index and optical thickness.

2. Thin film structure

The nm-layered thin film structure is shown schematically in Fig. 1. A homogeneous quarter wave layer with n = 2.09 is replaced by an optically equivalent stack of layers composed by pairs of nm-thick titania/silica layers (with titania being the first layer on top of a silicon substrate). We designed several prototypes with the number of layers ranging from 1 to 19. The corresponding layer thicknesses are shown in Table 1. All structures have the same total thickness of 127nm i.e. a quarter-wave optical thickness at 1064nm wavelength. The thickness ratio ρ of titania to silica is determined from Drude's formula:

$$\rho = \frac{n_H^2 - n_{eff}^2}{n_{eff}^2 - n_L^2} \tag{1}$$

The optical thickness *z* of the composite film (in units of the local wavelength), together with the minimum feasible thickness, also determines all optically equivalent composite designs differing for the number of nano-layers and their thicknesses $\delta_{L,H}$ via

$$N(\delta_L + \delta_H) = z\,\lambda_0 / n_{eff} \tag{2}$$

The layer thicknesses were measured from cross-sectional images of a transmission electron microscope.

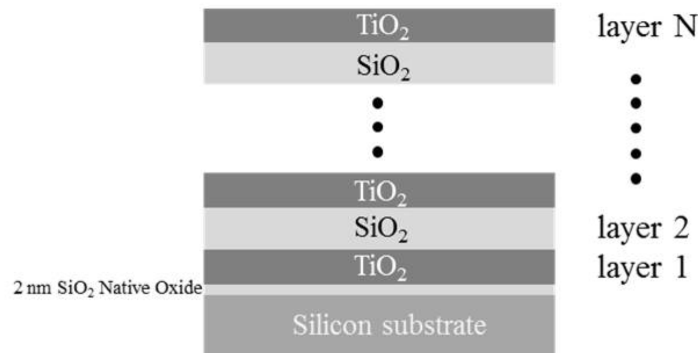

Fig. 1. Schematics of the nano-layer prototypes.

#224393 - $15.00 USD Received 6 Oct 2014; revised 8 Nov 2014; accepted 10 Nov 2014; published 20 Nov 2014
(C) 2014 OSA

Table 1. Thickness of the nano-layer prototypes.

Prototype	Designed thickness		Measured thickness	
	TiO_2(nm)	SiO_2(nm)	TiO_2(nm)	SiO_2(nm)
1-layer	127.27	–	121.90	–
3-layer	42.56(x2)	42.15(x1)	40.93(x2)	40.70(x1)
5-layer	28.37(x3)	21.07(x2)	27.09(x3)	19.83(x2)
7-layer	21.28(x4)	14.05(x3)	20.63(x4)	12.50(x3)
11-layer	14.19(x6)	8.41(x5)	13.68(x6)	7.44(x5)
15-layer	10.64(x8)	6.02(x7)	9.83(x8)	4.80(x7)
19-layer	8.51(x10)	4.68(x9)	7.36(x10)	4.32(x9)

3. Deposition

The substrate was a double-side-polished 10mm x 10mm square silicon chip, 500um in thickness with surface normal in the (100) direction. The silicon chip has a 2 nm thick native (glassy) oxide on the surface. We used a 2.5cm Kaufman type ion beam sputter apparatus for deposition. The deposition parameters are [24]: 1000V beam voltage, 50mA beam current and 200V accelerator voltage. A plasma bridge neutralizer was used to neutralize the ion beam. The sputter targets were high purity Ti and SiO_2 disks, 4” in diameter. They were thermally attached to either side of a water-cooled flat holder that could be flipped to face the incoming ion beam alternately, for depositing the titania and the silica layers. The coating chamber was pumped down to 10^{-6} torr for deposition. Oxygen gas was fed in the chamber with partial pressure of 10^{-4} torr for reactive sputtering. The angle of incidence of the ion beam was 45° to the target normal. The substrate holder was rotating on its axis. The surface normal of the substrate was perpendicular to the ion beam. The thickness uniformity of the coatings for both titania and silica was better than 96% within 5cm in diameter from the rotation axis. The thicknesses of the films were controlled by deposition time. Deposition rates for titania and silica films were calibrated in advance and appropriate deposition time were determined according to the design thickness. All samples were prepared and deposited under the exactly same rigorously controlled process conditions producing several prototypes for each type of geometry in Table 1. The prototypes were annealed in batch, and all prototypes with the same geometry gave consistent results in terms of their morphological and crystallization properties.

4. Thermal anneal

The samples were thermally annealed in air at different temperatures. During the anneal process, the temperature was initially ramped up at a rate of 3°C/min up to the desired level, and kept constant for 24 hours before the heating was turned off. The samples were then naturally cooled in the oven to room temperature. The time needed for cooling was approximately 24 hours. The temperatures chosen for our experiment were 225°C, 250°C, 300°C and 350°C. Based on our previous results with silica doped titania [1], we do not expect the loss angle to reduce dramatically upon further increasing the annealing temperature.

5. Transmission electron microscope

We used focused-ion-beam apparatus, model NOVA600 by FEI, to cut the nano-layer samples into ~50nm thick slices. A transmission electron microscope (TEM) was used to study the cross-section of the multi-layered slices. Electron diffraction patterns as well as high resolution images for the multi-layer stack were obtained. Thicknesses of the layers were measured from the TEM images because in the nano-meter scale TEM is more precise and reliable than conventional optical means such as ellipsometry, optical transmission spectrum or surface profile-meter.

6. X-ray diffraction

We used grazing angle x-ray diffraction to explore the crystal structures in the films. In this configuration, the x-rays were incident on the sample at an angle of 0.5°. Total external reflection occurs at the air-film interface because the refractive indices of the materials are smaller than that of air at the x-ray wavelength. X-rays propagate in the material only as an evanescent wave, and are scattered or diffracted by the near-surface layer structure. Therefore, most of the signal is from the films and little from the substrate. The detector scanned in the plane of incidence to record the diffracted and the scattered x-ray intensity as a function of 2θ where θ is the Bragg angle. For single crystal samples, such as the silicon wafer, only diffraction peaks that fall in the plane of incidence will be recorded. For poly-crystal samples, such as those forming in the multi-layers after anneal, full diffraction peaks will be recorded in the plane of incidence. The diffractometer we used was an X'Pert Pro MRD operated at the copper Kα line (1.5418A).

7. Results and discussion

7.1 Grazing angle X-ray diffraction results

The bare silicon substrates were checked first in order to reveal the background x-ray intensity distribution from the substrate and the instrument. The result is shown in the first pattern of Fig. 2(a). The other XRD patterns in Fig. 2(a) are for all samples before anneal. These patterns show only the characteristic broad peak of amorphous SiO_2 around 20° due to the amorphous silica layers and the background silicon signal. We conclude that the as-deposited titania layers in the nm-layer were amorphous in structure. This observation is consistent with previously reported results for pure titania films deposited on soda lime glass substrates under the same deposition condition [1,7].

Figure 2(b), 2(c), and 2(d) show the XRD patterns for the samples after annealing at 225°C, 250°C and 300°C, respectively. Figure 2(e) shows the XRD pattern of the 19-layers sample annealed at 350°C. On top of each figure, the standard XRD distribution of the crystalline anatase phase of TiO_2 from the JCPDS 84-1286 database is shown. The observed XRD patterns match that of the standard database. It is clear that the titania layers in the nm-layer structure crystallized into anatase phase of TiO_2 upon annealing.

The strongest diffraction peak (101) of the anatase phase for 5-layer sample annealed at 225°C and for the 19-layer sample annealed at 300°C were faint, they can barely be seen in Fig. 2(b) and 2(d). We have fitted these two faint peaks to a Gaussian distribution and the close-up results of the fittings are shown in Fig. 2(f) and 2(g). The amplitudes of the (101) peaks are small but, however, distinguishable from the background noise as shown in the figures. If we define the criterion for onset of crystallization as the amplitude of the (101) x-ray diffraction peak starts to be distinguishable from the rms background noise, then the threshold temperatures for the 5-layer and the 19-layer samples should be near 225°C and 300°C, respectively.

Table 2. Summary of the crystallization results of Fig. 2.

Prototype	Before annealing	225°C 24hr	250 °C 24hr	300 °C 24hr	350 °C 24hr
1 layer	No	No	Yes	Yes	–
3 layer	No	Yes	Yes	Yes	–
5 layer	No	Thr*	Yes	Yes	–
7 layer	No	No	Yes	Yes	–
11 layer	No	No	Yes	Yes	–
15 layer	No	No	No	Yes	–
19 layer	No	No	No	Thr*	Yes

* Thr: threshold, see Fig. 2(f) and 2(g) with the preceding statements.

Table 2 summarizes the pictorial results of Fig. 2. As-deposited amorphous titania layers ultimately crystallized after thermal annealing, and that the XRD patterns of the crystallites coincide with that of the anatase TiO_2 phase. The general trend is that there is a threshold annealing temperature for the onset of crystallization, which increases with increasing number of layers, or equivalently, with decreasing the (titania) layer thickness.

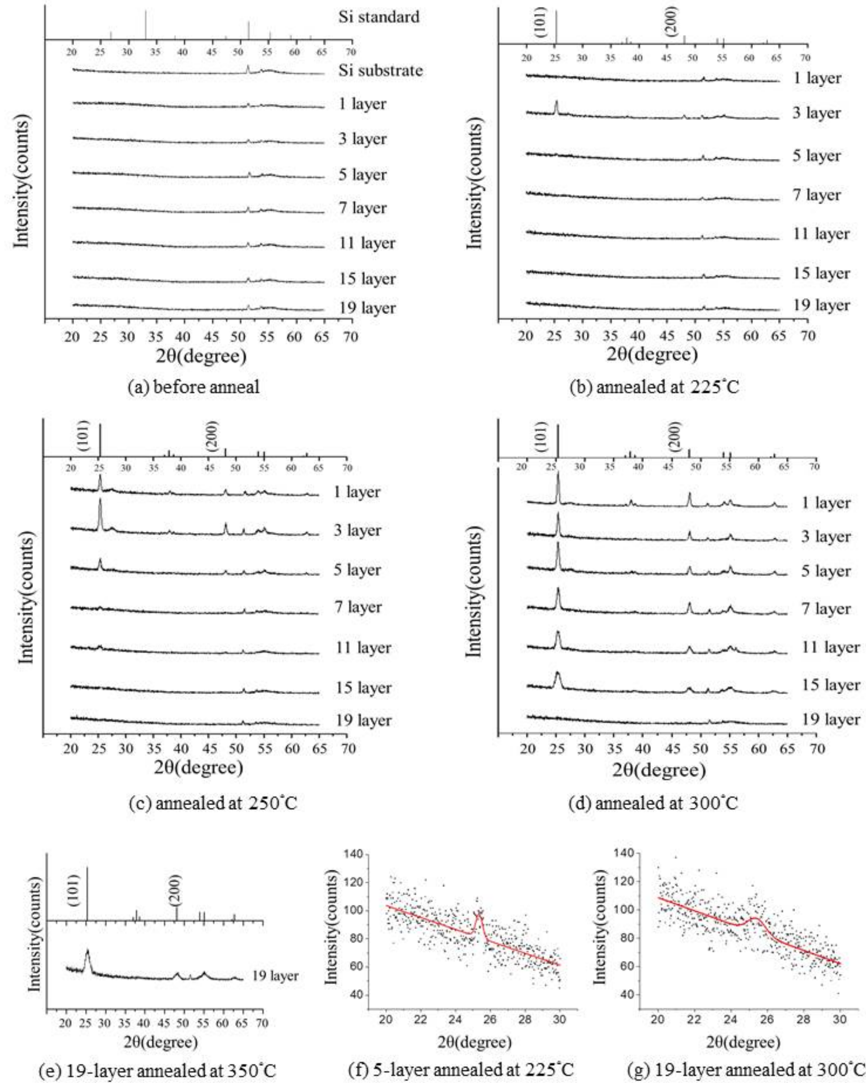

Fig. 2. Grazing angle x-ray diffraction pattern of all samples subjected to anneal at various temperatures (a) before anneal, (b) 225 °C, (c) 250°C, (d) 300 °C, (e) 350 °C for 19-layer prototype, (f) 225 °C for 5-layer prototype and (g) 300°C for 19-layer prototype.

Contrary to the general trend in Table 2, crystallization in the 1-layer (a single titania layer with 127 nm thickness) samples occurred at a higher temperature, compared to the 3-layer samples. A basic difference between the monolayer and the multilayers is that in the former titania is deposited on crystalline silicon, while in the latter all titania layers, except for the bottom one, are deposited on silica. Silicon has a much larger thermal conductivity than silica, apt to rapidly quench the localized temperature pulses due to impinging atoms/clusters in the deposition stage. Fast quenching depresses the diffusion processes at the base of nucleation.

#224393 - $15.00 USD Received 6 Oct 2014; revised 8 Nov 2014; accepted 10 Nov 2014; published 20 Nov 2014
(C) 2014 OSA

We speculate that reduced nucleation in the deposition stage due to rapid quenching may leads to retardation of the crystallization in the post-deposition annealing, and that explains the observed anomaly for the 1-layer sample. Single layer titania film, with thickness of 380nm, deposited on soda-lime glass substrates (75% SiO_2) under the same deposition and annealing conditions as in this experiment [1,7], however, did crystallize at lower temperature of 200°C~225°C that is consistent with the general trend of this observation.

7.2 TEM investigation

Figure 3 shows cross-sectional images and electron diffraction patterns of the 1-, 3-, 15-, and 19-layer samples before and after annealing at 300°C. The lighter, structure-less layers are the silica layers that are amorphous in all samples both before and after anneal. The darker layers in the 1-, 3-, and 15-layers samples before anneal, and in the 19-layers sample before and after anneal are also structure-less, i.e. titania in the amorphous state. As an added confirmation, these layers produced diffused electron diffraction patterns. Note that onset of crystallization for the 19-layer samples at 300°C, as revealed in the x-ray diffraction, did not produce noticeable changes in the electron diffraction and direct image of the amorphous phase. Close-up view of the images for 1-, 3-, and 15-layers samples after 300°C anneal clearly reveal both the lattice structure of the anatase crystallite and the electron diffraction patterns of the poly-crystals.

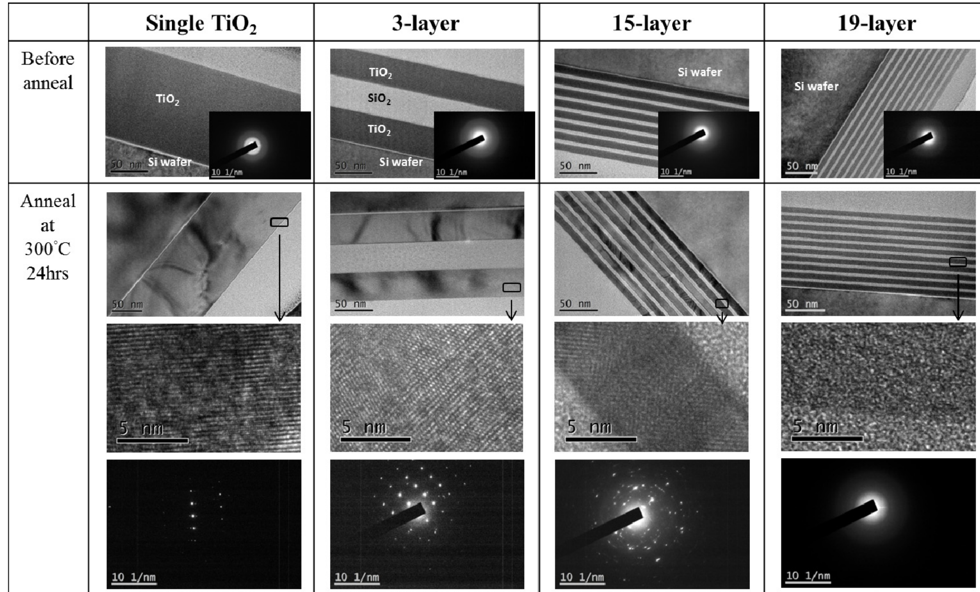

Fig. 3. TEM images and electron diffraction patterns of the samples.

The observed behavior (namely, that nm-layered silica/titania composites with thinner layers crystallize at higher annealing temperatures) is fully consistent with known results [21,22]. This has been related to the increasing role of surface energy with decreasing film thickness. In our nm-layered samples, the glass-forming silica layers help suppressing the growth of nuclei into crystallites at the interfaces, with increasing effectiveness as the area-to-volume ratio increases with decreasing titania film thickness.

8. Conclusion

A thickness dependent threshold temperature for the crystallization of the titania films is observed in multi-layer stacks of nm-thick titania/silica pairs deposited by ion beam sputter method. Thinner titania layers show higher threshold temperature of crystallization. The

#224393 - $15.00 USD Received 6 Oct 2014; revised 8 Nov 2014; accepted 10 Nov 2014; published 20 Nov 2014
(C) 2014 OSA

amorphous high index layers of HR optical coatings could be thus replaced by a nano-layer composite. The optical index of the composite can be finely tuned in the range 1.46 to 2.32 between the indexes of the two materials. The higher temperature anneal possible is expected to produce lower mechanical losses, and hence lower thermal noise. It is expected that this advantage will persist in the cryogenic regime where 3rd generation laser interference gravitational wave detectors will operate.

Acknowledgment

Fruitful discussions with G.M. Harry, I. Martin, R. Nawrodt, S. Penn and the Coating Group of the LIGO Scientific Collaboration is gratefully acknowledged. This work has been sponsored in part by the National Science Council of Taiwan, R.O.C. under the project NSC-100-2221-E-007-099 and by the Italian Institute for Nuclear Physics under the MIDI-BRUT and AdCOAT grants (INFN-CSN V).